Prototypes of Nonrelativistic Spin Splitting and Polarization in Symmetry Broken Antiferromagnets

Xiuwen Zhang,[1,*,†] Jia-Xin Xiong,[1,*] Lin-Ding Yuan,[2] and Alex Zunger[1,‡]

[1]*Renewable and Sustainable Energy Institute, University of Colorado, Boulder, Colorado 80309, USA*
[2]*Department of Materials Science and Engineering, Northwestern University, Evanston, Illinois 60208, USA*

(Received 4 October 2024; revised 1 May 2025; accepted 21 July 2025; published 25 September 2025)

Antiferromagnets that break both space-time reversal and translation-spin-rotation symmetries were recently predicted [L.-D. Yuan, Z. Wang, J.-W. Luo, E. I. Rashba, and A. Zunger, Phys. Rev. B **102**, 014422 (2020)] to possess splitting between the otherwise spin-degenerate energy bands even without the relativistic spin-orbit coupling (SOC). Here, we point out that such nonrelativistic spin splitting (NRSS)—in particular, "spin splitting type 4" (SST-4) symmetry-broken antiferromagnets—can be divided into subgroups having distinct patterns of spin splitting and spin textures, depending on additional auxiliary symmetries of spin interconversion and polarity. These SST-4 subgroups include the α-type (no spin-interconverting symmetry) having spin splitting at the Brillouin zone center, as well as the β subgroup in which a rotation symmetry is applied and determines the alternating spin texture and the γ subgroup having exclusively reflection spin-interconverting symmetry. Unlike ferrimagnets, the α-type compounds are shown to have tiny net magnetization at finite temperature and thus avoid the adverse effect of the stray field. The α and β subgroups can be either polar or nonpolar, whereas the γ subgroup is polar only, providing a basis for possible switching by external fields. The combination of NRSS-enabling and auxiliary symmetries is used here as a filter for identifying previously synthesized compounds as specific prototypes. Their characteristic splitting and spin polarization are calculated by density functional theory to the benefit of potential future experimental testing. Interesting results are as follows: (i) SOC-independent NRSS can exceed the magnitude of the SOC-induced Rashba and Dresselhaus spin splitting in semiconductors. (ii) Examples of predicted α-type insulating compounds include $BiCrO_3$ (nonpolar) and Mn_2ScSbO_6 (polar), the latter having spin splitting of 158 meV and 160 meV in the valence and conduction bands, respectively. (iii) The β-type ($Cu_2Y_2O_5$ and FeF_2) and γ-type compounds ($Mn_4Nb_2O_9$ and $FeScO_3$) are distinguished both by their auxiliary symmetries and polarity. The spin textures of γ-type compounds are mirror reflected with spin degeneracy of the wave vectors on that mirror. These observations will likely broaden the experimental playing field of NRSS physics significantly.

DOI: 10.1103/mrzv-wmcf

Subject Areas: Condensed Matter Physics, Materials Science, Spintronics

I. INTRODUCTION

The removal of the degeneracy between quantum states of matter has long established a route for deeper appreciation of what leads to such degeneracies in the first place and how removal of the degeneracy can be exploited to create spin polarization and to transport spin current. Orbital degeneracy removal entails atomic-scale structural symmetry breaking [1–3]. Kramer's (spin) degeneracy removal, as in the Zeeman effect, requires the presence of a nonzero net magnetization, as in ferromagnetic or ferrimagnetic systems with broken time-reversal symmetry. In nonmagnetic materials, spin degeneracy can be lifted by broken inversion and relativistic spin-orbit coupling (SOC), as in the Rashba or Dresselhaus effects [4–6]. Such splitting of spin bands requires the presence of (a) SOC in (b) nonmagnetic systems, with (c) broken inversion symmetry (noncentrosymmetric compounds). The question of whether spin degeneracy removal could be possible (a') without SOC, in (b') magnetic systems, (c') even with unbroken inversion symmetry in the most general situation, has been

*These authors contributed equally to this work.
†Contact author: xiuwen.zhang@colorado.edu
‡Contact author: alex.zunger@colorado.edu

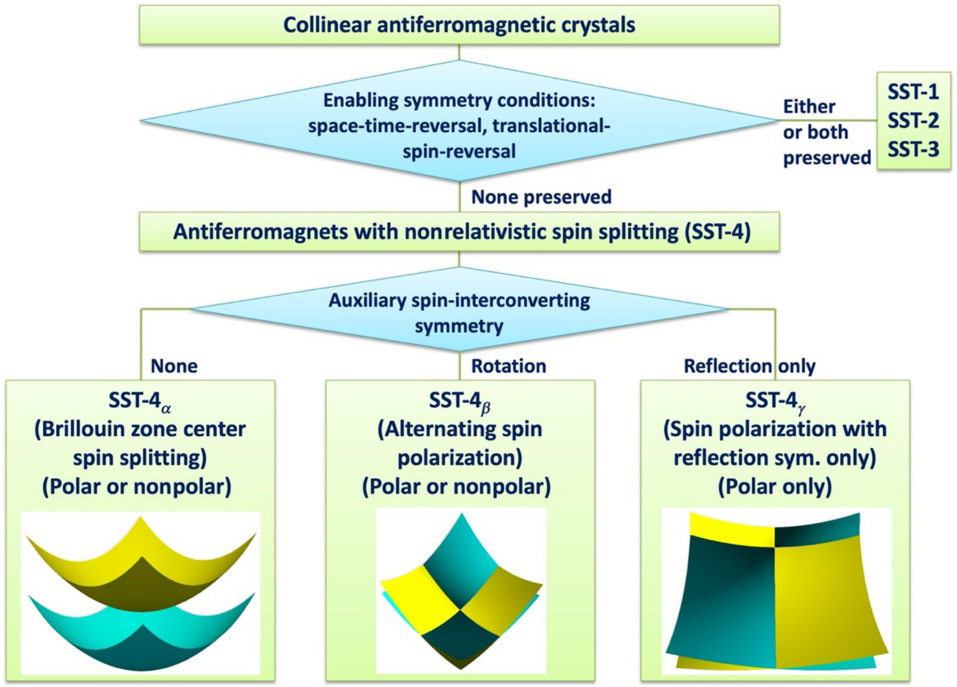

FIG. 1. Subgroups of collinear antiferromagnets with different prototypes of nonrelativistic spin splitting and spin polarization. The two surfaces in the bottom panels represent the spin-up (gray) and spin-down (blue) bands. Considering polar symmetry, there are polar and nonpolar subgroups for each of the SST-4_α and SST-4_β prototypes of NRSS antiferromagnets. SST-4_γ can only be polar.

raised in different ways in the past [7–18]. Such nonrelativistic spin splitting (NRSS) independent of SOC (the mass-velocity term and the Darwin term of the relativistic corrections [19] do not lead to the spin splitting) would be interesting—not only because it significantly broadens the playing field of magnetic materials to include spin-split antiferromagnetic (AFM) energy bands but also because it frees one from the need to employ compounds with heavy atoms having strong SOC, with their weaker chemical bonds (e.g., Hg-Te vs Zn-O [20–22]), prone to defect formation. Furthermore, low SOC compounds could have spin-polarized bands with a longer carrier lifetime as in silicon [23].

The possibility of SOC-independent spin-degeneracy removal pointed out in 1964 by Pekar and Rashba due to the spontaneous inhomogeneous magnetic field in antiferromagnets [7]. However, this pioneering idea did not lead to the formulation of the enabling conditions of NRSS. Whereas some of the AFM materials studied since then most likely had NRSS fingerprints (such as MnO_2 [24], FeF_2 [18], and RuO_2 [11]), at the time, they were not recognized as SOC-independent. The subject of discovery of NRSS-enabling conditions lay dormant for another half a century. Naka *et al.* [9] noted the spin splitting in a class of organic antiferromagnetic compounds without SOC. Hayami *et al.* found the same SOC-unrelated momentum-dependent spin splitting effect in AFM materials and studied the conditions enabling the effect in collinear antiferromagnets [10].

A deliberate symmetry-based search of real materials hosting NRSS can be performed by applying appropriate symmetry-breaking conditions to the traditional (i.e., spin unsplit) Néel antiferromagnets and then searching for material realizations that satisfy such enabling conditions. The results of such an "inverse design" search [25] (given the target spin property, search the materials having it) are then validated by energy-minimizing electronic structure theory and experiment. Examples of such magnetic inverse design are given in Ref. [26]. Symmetries that enable NRSS when broken were identified in AFM compounds by Yuan *et al.* in collaboration with Rashba *et al.* [8]. Using these NRSS-enabling conditions opened the way for the symmetry-guided material search of spin-split AFM compounds, which were previously synthesized but not identified as NRSS AFM compounds. Such identification was validated via density functional theory (DFT) [27–29] band structure calculations, excluding the SOC term in the Hamiltonian [26].

A. Two enabling symmetries and SST classifications of compounds

The symmetry conditions require both (i) the breaking of the ΘI space-time-reversal symmetry, which is a product of time reversal (Θ) with inversion (I), and (ii) the breaking of UT translational-spin-rotation symmetry, which is a product of a $SU(2)$ spin rotation (U) that reverses spin with

TABLE I. Base spin-splitting types defined [8,26] by whether the ΘI space-time-reversal symmetry and the UT translational-spin-reversal symmetry are both broken (leading to SST-4) or only partially broken (leading to SST-1 and SST-3) or both preserved (SST-2). The enabling symmetry is described in both the MSG and the MPG. The last two columns also show whether each SST can be CS or non-CS, and polar or nonpolar. SST-1, 2, 3, and 4 exist in antiferromagnets. SOC is needed for SST-3 but not for SST-4 to induce spin splitting.

Spin-splitting type	Magnetic space group		Magnetic point group				
	Having ΘI	Having UT	Having ΘI	Having Θ	CS or non-CS	Polar or nonpolar	Spin splitting
SST-1	Yes	No	Yes	No	CS	Nonpolar	No
SST-2	Yes	Yes	Yes	Yes	CS	Nonpolar	No
SST-3	No	Yes	No	Yes	CS/non-CS	Polar/nonpolar	Yes (SOC-induced)
SST-4	No	No	No	No	CS/non-CS	Polar/nonpolar	Yes (NRSS)

a fractional translation (T). In collinear AFM compounds, there exists ΘU symmetry; therefore, the existence of UT also implies the existence of ΘT (type IV magnetic space group). These enabling symmetries can be described by two equivalent symmetry languages: the magnetic space group (MSG) [26] or the magnetic point group (MPG). The ΘI symmetry in MSG has the same form in MPG, and UT symmetry in MSG is equivalent to the time-reversal symmetry Θ in MPG. Note that, in addition to the two NRSS-enabling symmetries (i) and (ii), in two-dimensional system, broken twofold rotation and mirror-reflection symmetry are also required [30,31].

The presence or absence of the two enabling symmetries (i) and (ii) gives rise to four "spin splitting types" (SST) in AFM compounds: SST-1, SST-2, SST-3, and SST-4. The AFM compounds belonging to SST-1, 2, and 3 have no double symmetry breaking, thus no spin splitting without SOC, whereas SST-4 AFM materials have (broken ΘI, broken UT) = (Yes, Yes), hence producing NRSS. Figure 1 and Table I show the "family tree" of the AFM compounds. The present description includes the information of the presence or absence of spatial inversion symmetry and polarity for each spin-splitting type: SST-1 and 2 are centrosymmetric (CS) and nonpolar, whereas SST-3 and 4 can be either CS or non-CS and thus can be polar.

The classification of SST-1, 2, 3, and 4 identifies materials with given symmetries and properties. A few examples shown as follows: The SST-1 class (no spin splitting) includes CuMnAs, $MnGeO_3$, and Ca_2MnO_4; SST-2 (no spin splitting) includes NiO and $FeBr_2$; SST-3 that has spin splitting but is only SOC induced, is exemplified by MnS_2 and $AgNiO_2$ [26]. In contrast, SST-4 has spin splitting even without SOC. It is exemplified by MnF_2, $LaMnO_3$, and $MnTiO_3$ [26]. We mention in passing that a material classification that maps into the above SST classification was recently given [32], where "FM" or "M-type altermagnets (AM)" are ferromagnets and ferrimagnets; unbroken AFM includes SST-1 and SST-2; "A-type AM" is SST-3; "S-type AM" is centrosymmetric SST-4; and "S/A-type AM" is noncentrosymmetric SST-4. The classification of the physical crystals into SST classes is different than the spin Laue group classifications [14] that discuss reciprocal-space symmetries of specific wavefunctions $\psi(n,k)$ in a given band (n) and a given SST-I (I = 1, 2, 3, 4) material (see Supplemental Material [33], Sec. I).

B. Breaking SST-4 into subgroups α, β, γ

We analyze the primary nonrelativistic (SST-4) spin-split antiferromagnets, depending on the application of additional, auxiliary, spin-interconverting symmetry conditions that connect the two spin-opposite sublattices. We break the SST-4 into different subgroups, as illustrated by the last two lines of Fig. 1. Auxiliary symmetry conditions do not affect the very existence of NRSS but lead to different prototypic spin splitting and spin textures. SST-4_α is a subgroup that has no spin-interconverting symmetry but is constrained by identical number of spin-opposite occupied electrons to have zero magnetization at $T = 0$ and almost zero total magnetization under perturbed filling conditions. This case will be illustrated in Sec. IV E. As such, α-type materials are not compensated ferrimagnets with rapidly increasing magnetization as a function of perturbations in level filling. When the spin-interconverting symmetry is rotation, we refer to this subgroup as SST-4_β, which includes altermagnets, such as MnF_2. When the spin-interconverting symmetry is exclusively reflection (without any rotation), we refer to this subgroup as SST-4_γ. Note that α- and β-type materials can be either polar or nonpolar. Unlike β-type materials, the γ-type materials can only be polar. The β- and γ-type materials were previously [14] lumped together under the title "altermagnets," but the distinctions of defining symmetries and the resulting electronic properties were not revealed. These distinctions will be discussed in Sec. IV D. Here, we study the different spin splitting, spin texture, and metal-vs-insulator properties for these SST-4 subgroups, as schematically shown in the last row of Fig. 1. Some of the main points are as follows:

(a) Material realizations of the NRSS subgroups of SST-4 are predicted via constraining specific symmetries and then searching candidate compounds in databases, followed by validation of fingerprint properties via

DFT calculations. As such, they are prime candidates for experimental studies of spin-split AFM compounds.

(b) The spin splitting at the Brillouin zone center in α-type compounds (reminiscent of ferromagnetic materials) has only tiny nonzero net magnetization under occupation perturbations and thus avoids the adverse effect of the stray field.

(c) The α-type compounds are insulators (or half-metals), while the β-type and γ-type compounds can be either insulators, semimetals, or metals.

(d) The β-type and γ-type compounds are distinguished both by their auxiliary symmetries and polarity. The γ-type compounds can only be polar, while the β-type compounds can be both polar and nonpolar. The spin textures of γ-type compounds are mirror reflected with spin degeneracy at the wave vectors on that mirror reflection plane.

II. IDENTIFICATION OF AUXILIARY SYMMETRIES

In addition to the NRSS-enabling symmetries that break both space-time-reversal and translation-spin rotation symmetries in collinear bulk AFM materials, there can be additional spin-interconverting auxiliary symmetries that do not influence the very existence of NRSS but have impacts on other properties. These auxiliary symmetries can be polar vs nonpolar symmetries and can connect the spin-opposite sublattices in AFM compounds. Particularly, the spin polarization in polar SST-4 materials has the potential to be switched by external electric fields [34].

A. Identification of auxiliary symmetries that are magnetically polar or nonpolar

Polar magnetic symmetry means a symmetry that allows a spontaneous electric polarization in the magnetic systems. The polar magnetic symmetry has the potential for possible applications in field switching and can be described either by MSG or MPG. The MPGs that include the information of inversion symmetry and polarity in SST-1, 2, 3, and 4 are listed in Table II. Polar AFM compounds can only appear in SST-3 and 4, not in SST-1 and 2.

B. Identification of auxiliary symmetries that are spin-interconverting

The symmetry operations of the magnetic ion Wyckoff positions in the crystallographic space group plus the direction of the magnetic moments can be used to identify the auxiliary symmetries of spin-interconverting symmetries. Spin-interconverting symmetries connect the spin-opposite sublattices and enforce the local magnetic moments to be compensated in collinear AFM materials. Enabling spin-interconverting symmetries (ΘI and UT) determine the existence of NRSS effects. Here, we focus on the other, auxiliary spin-interconverting symmetries that do not affect the existence of NRSS but shape the spin-splitting properties of the AFM compounds with NRSS (SST-4). As shown in Fig. 1, we define three subgroups based on the spin-interconverting auxiliary symmetries: The α subgroup has no spin-interconverting symmetries with the (nearly) zero total magnetization robust against external perturbations; the β subgroup has spin-interconverting symmetries that include rotation operations with optional reflection symmetries; the γ subgroup has spin-interconverting symmetries that exclusively include the reflection symmetries without any rotation symmetries. Given that different Wyckoff positions are generally not interchangeable, there are three cases for the positions of magnetic ions: (i) Same-element ions are geometrically equivalent when located at the same Wyckoff position; (ii) same-element ions are geometrically inequivalent when located at different Wyckoff positions, where every

TABLE II. Magnetic point groups (MPGs) for four SST in collinear AFM compounds, including the presence or absence of polarity. The 16 nonpolar MPGs that exist in cubic crystals are not listed because they are not collinear.

Spin-splitting type	Polar or nonpolar MPG	Magnetic point group	Number of MPG
SST-1	Nonpolar	[−1′]; [2′/m]; [2/m′]; [m′mm]; [m′m′m′]; [4/m′]; [4′/m′]; [4/m′mm]; [4′/m′m′m]; [4/m′m′m′]; [−3′]; [−3′m]; −[3′m′]; [6′/m]; [6/m′]; [6/m′mm]; [6′/mmm′]; [6/m′m′m′]	18
SST-2	Nonpolar	[−11]; [2/m1′]; [mmm1′]; [4/m1′]; [4/mmm1′]; [−31′]; [−3m1′]; [6/m1′]; [6/mmm1′]	9
SST-3	*Polar*	[**11′**]; [**m1′**]; [**21′**]; [**mm21′**]; [**41′**]; [**4mm1′**]; [**31′**]; [**3m1′**]; [**61′**]; [**6mm1′**]	10
	Nonpolar	[2221′]; [−41′]; [4221′]; [−42m1′]; [321′]; [−61′]; [6221′]; [−6m21′]	8
SST-4	*Polar*	[**1**]; [**2**]; [**2′**]; [**m**]; [**m′**]; [**mm2**]; [**m′m2′**]; [**m′m′2**]; [**4**]; [**4′**]; [**4mm**]; [**4m′m′**]; [**4′m′m**]; [**3**]; [3**m**]; [**3m′**]; [**6**]; [**6′**]; [**6mm**]; [**6m′m′**]; [**6′mm′**]	21
	Nonpolar	[−1]; [2/m]; [2′/m′]; [222]; [2′2′2′]; [mmm]; [m′m′m]; [−4]; [−4′]; [4/m]; [4′/m]; [422]; [42′2′]; [4′22′]; [−42m]; [−42′m′]; [−4′2′m]; [−4′2m′]; [4/mmm]; [4/mm′m′]; [4′/mm′m]; [−3]; [32]; [32′]; [−3m′]; [−3m]; [−6]; [−6′]; [6/m]; [6′/m′]; [622]; [62′2′]; [6′22′]; [−6m2]; [−6m′2′]; [−6^{2}m2′]; [−6′m′2]; [6/mmm]; [6′/m′mm′]; [6/mm′m′]	40

Wyckoff position has both spin-up and spin-down magnetic moments; (iii) same-element ions are geometrically inequivalent when located on different Wyckoff positions, where every Wyckoff position only has spin-up or spin-down magnetic moments. We then check the auxiliary spin-interconverting symmetry operations for the three cases listed above: For case (i), we check whether any rotation or reflection operations, except for those operations included in the Wyckoff position, can connect the spin-opposite magnetic ions; for case (ii), we check whether any rotation or reflection operations, except for those operations included in every Wyckoff position, can connect the spin-opposite magnetic ions on the same Wyckoff position; for case (iii), there will be no auxiliary symmetry in this compound. The ligand nonmagnetic atoms are automatically paired by these auxiliary symmetries. The above analysis is equivalent to the symmetry analysis in the magnetic space group that includes direction of magnetic moments. Based on the examination result of either case, we can identify the following subgroups:

Identification of α-type compounds: The compound belongs to case (i) or case (ii), and there is no rotation or reflection operations connecting spin-up and spin-down magnetic ions. Otherwise, the compound belongs to case (iii).

Identification of β-type compounds: The compound belongs to case (i) or case (ii) but not to case (iii), and there is at least one rotation operation connecting spin-up and spin-down magnetic ions.

Identification of γ-type compounds: The compound belongs to case (i) or case (ii) but not to case (iii), and the operation connecting spin-up and spin-down magnetic ions is exclusively reflection symmetry without any rotation symmetry.

As an illustration of the auxiliary spin-interconverting symmetry identification process, in the polar β-type material $Cu_2Y_2O_5$ with space group $Pna2_1$ and magnetic space group $Pna2_1$, the magnetic ions Cu^{2+} are located on two sets of $4a$ Wyckoff positions. We find that the symmetry operations $\{2_{001}|0,0,\frac{1}{2}\}$ and $\{m_{100}|\frac{1}{2},\frac{1}{2},\frac{1}{2}\}$ can interconvert the spin-up and spin-down Cu^{2+} ions along the y direction. Thus, we identify two spin-interconverting auxiliary symmetries in $Cu_2Y_2O_5$: the twofold screw axis 2_1 along the c axis (z axis) of the crystal and the glide reflection n with the mirror plane perpendicular to the a axis (x axis). The spin-interconverting auxiliary symmetries can also be indicated by the magnetic space group without SOC. For instance, we find that the magnetic space group without SOC of $Cu_2Y_2O_5$ is $Pn'a2'_1$, which indicates the two spin-interconverting auxiliary symmetries $2'_1$ and n'.

C. Combining magnetically polar and spin-interconverting symmetries produces five SST-4 subgroups

Considering the two types of auxiliary symmetries in collinear AFM materials, i.e., polar vs spin-interconverting auxiliary symmetries, there are five subgroups in total: Both the α and β subgroups can either be polar and nonpolar, but the γ subgroup can only be polar. The forbidden nonpolarity in the γ subgroup can be explained as follows.

For a γ-type material to be nonpolar, one needs three mirror planes (associated with reflectional symmetries) perpendicular to each other. If one or three reflectional symmetries were spin interconverting, ΘI would be an operation of the magnetic space group and the material would not have the NRSS effect [8], which is not possible for γ-type systems. If two of the reflectional symmetries were spin interconverting, then $4'_x$, $4'_y$, or $4'_z$ or their related symmetries with translations would be operations of the magnetic space group, in which case the system would belong to β-type materials. Therefore, γ-type materials can only be polar.

III. APPROACHES FOR ELECTRONIC STRUCTURE AND SYMMETRIES WITH OR WITHOUT SPIN-ORBIT COUPLING

The materials identified by symmetry conditions are validated by performing DFT calculations connecting the symmetry conditions to material properties. The SST-4 material examples are identified from the MAGNDATA database [35] based on the analysis of the NRSS-enabling symmetry conditions. Literature on other synthesized AFM compounds that have the same symmetry as the AFM compounds in MAGNDATA [35] provides additional identifications. For each compound, MAGNDATA [35] gives the crystal structure, magnetic configuration, and experimental reference about the synthesis method and magnetic ordering properties such as Néel temperature (T_N). The calculations for representative materials of each subgroup are done by DFT [27–29] with the Perdew-Burke-Ernzerhof (PBE) exchange-correlation functional [36] and the on-site electronic Coulomb correlation term U [37–39] (see Supplemental Material [33], Sec. II).

There are two main approaches for symmetry analysis for collinear magnets: (i) MSG (or MPG) without SOC [40], which is equivalent to the spin space group [41,42] (or spin point group), and (ii) MSG [8] (or MPG), which is the crystallographic space group (or point group) plus the direction of magnetic moments. Approach (i) assumes that the direction of local magnetic moments has no impact on the magnetic symmetry and physical properties, i.e., spin and space degrees of freedom are decoupled; approach (ii) includes the direction of local magnetic moments that could have an impact on magnetic symmetry as well as physical properties. Both approaches (i) and (ii) can be used; however, approach (i) assumes no directional moment configurations, whereas approach (ii) uses the magnetic space groups (or point groups) with given directions of magnetic moments for symmetry analysis in collinear magnets. Like approach (ii), DFT generally does not assume

TABLE III. Examples of predicted subgroups of SST-4 materials: literature synthesis method, magnetic ordering, space groups, magnetic space groups, magnetic point groups, SST-4 subgroup, and prototypic spin property of different subgroups of SST-4 materials. The compounds with cross substitutions of atomic sites on Wyckoff positions of the crystallographic space groups are indicated by stars.

Material	Synthesis method	Magnetic ordering	SG/MSG/MPG	NRSS subgroup	Spin property
$BiCrO_3$	High-pressure–high-temperature solid-state reaction[a]	AFM with $T_N = 110$ K[a]	*C2/c*; *C2/c;* *2/m*	Nonpolar α type	Brillouin-zone-center spin splitting
Mn_2ScSbO_6*	High-pressure–high-temperature synthesis[b]	AFM below $T_N = 22.3$ K[b]	*R3*; *P1;* *1*	Polar α type	Potentially electrically switchable Brillouin-zone-center spin splitting
$Cu_2Y_2O_5$	Solid-state reaction[c]	AFM with $T_N = 13$ K[c]	$Pna2_1$; $Pna2_1$; *mm2*	Polar β type	Potentially electrically switchable alternating spin polarization in the plane perpendicular to the polar axis
FeF_2	Grown from the melt[d]	AFM at 78 K with the opposing moments aligned along the *c* axis[e]	$P4_2/mnm$; $P4'_2/mnm'$; $4'/mm'm$	Nonpolar β type	Alternating spin polarization
$Mn_4Nb_2O_9$	Solid-state reaction[f]	AFM below $T_N = 109.1$ K[g]	*Cc*; *Cc;* *m*	γ type	Potentially electrically switchable spin polarization with reflection symmetry and mirror planes parallel to the polar axis
$FeScO_3$*	Conventional solid-state methods[g]	AFM at 300 K with antiparallel spins for all nearest neighbors[f]	*R3c*; *Cc′*; *m′*	γ-type	Potentially electrically switchable spin polarization with reflection symmetry and mirror planes parallel to the polar axis

[a]Ref. [43].
[b]Ref. [44].
[c]Ref. [45].
[d]Ref. [46].
[e]Ref. [47].
[f]Ref. [48].
[g]Ref. [49].

lack of directionality of the magnetic moments. The degree to which directionality is important in different compounds is an open question. Here, we use the more general approach (ii) for the symmetry analysis. For completeness, we also discuss approach (i) in Sec. IV E. The compounds discussed in this paper (Table III and Figs. 2–7) have the same classification in either approach (i) or (ii).

IV. PREDICTED SYNTHESIZABLE COMPOUNDS OF SST-4 SUBGROUPS

In this section, we provide our DFT results for material examples of α-, β-, and γ-type SST-4 subgroups (see Table III). In Secs. IVA–IVC, we show the electronic structures including band gap and spin polarizations for the AFM materials at zero temperature. We discuss the distinction between β- and γ-type materials in Sec. IV D. In Sec. IV E, we use the MPG without SOC for classifying SST-4 subgroups to compare with the classifications using MPG. In Sec. IV F, we investigate the total magnetization as a function of external perturbations. In particular, we discuss how compensated ferrimagnets differ from the α-type AFM materials.

A. SST-4$_\alpha$ subgroup: Absence of spin-interconverting auxiliary symmetry and the resulting Brillouin-zone-center spin splitting for polar or nonpolar systems

The most important feature of α-type AFM compounds is the Brillouin-zone-center spin splitting, which is due to the absence of any spin-interconverting auxiliary symmetry. Yet, the total magnetic moment of the crystal is compensated to zero at zero temperature. For well-designed insulating α-type compounds, the total magnetization is finite but vanishingly small, for example, $BiCrO_3$ and Mn_2ScSbO_6. This total magnetization can be explained by the identical number of occupied spin-up and spin-down valence electrons, which are "filling-enforced" [51,52]. The DFT results show that the total magnetizations in $BiCrO_3$ are zero at zero temperature and 0.0001 μ_B at the effective temperature of 2000 K. We will discuss the details of the total magnetization in α-type AFM as a function of external perturbation as a broad subject in Sec. IV D.

The MPG of $BiCrO_3$ is *2/m*, where neither 2_y nor m_y operations can interconvert the magnetic moments along the *y* direction; thus, there is no spin-interconverting

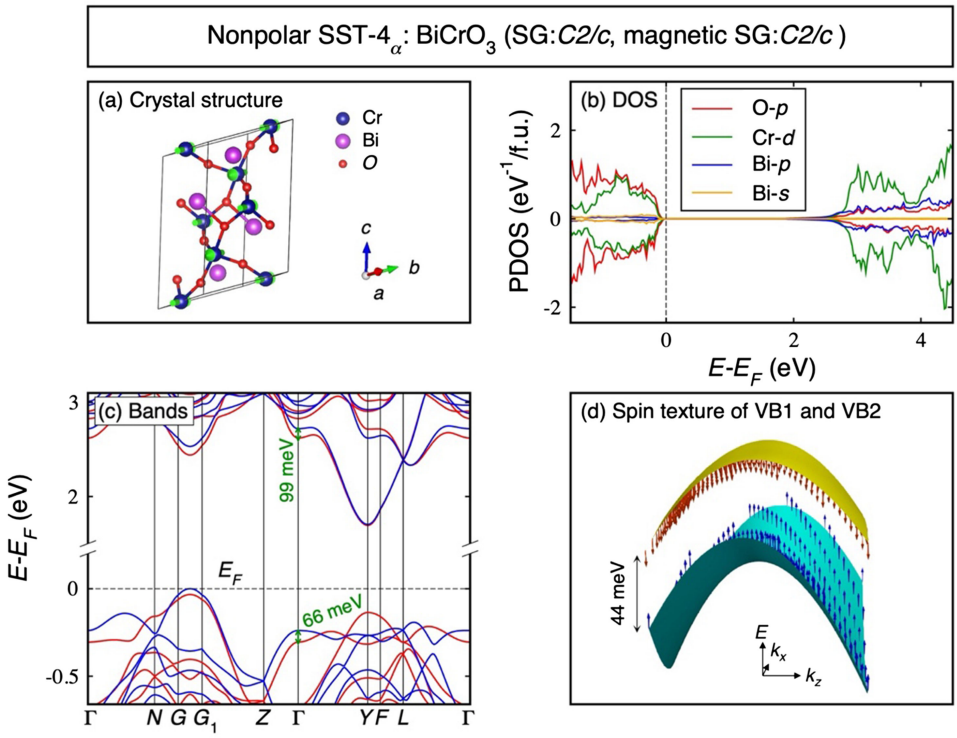

FIG. 2. Nonrelativistic (SOC = 0) spin splitting in nonpolar α-type antiferromagnet $BiCrO_3$ (space group: *C2/c*, magnetic space group: *C2/c*). (a) Crystal structure drawn by using the VESTA software [50]. (b) Partial density of states. (c) Band structure. Red (blue) curves in the band structure: spin-up (spin-down) polarized bands. The spin-splitting energies between the first two conduction bands and the first two valence bands at the Γ point, respectively, are indicated by green arrows. (d) Spin texture of the first and second valence bands in the (010) plane perpendicular to the magnetic moments around the Γ point. The magnetic moments and spin polarization are along the y axis (b axis of the monoclinic unit cell). The range of $k_x(k_z)$ in the spin texture plot is $(-0.02, 0.02)$ $2\pi/\text{Å}$.

symmetry to protect the spin degeneracy at any k point in $BiCrO_3$. Spin splitting prevails in the whole Brillouin zone, including the Brillouin zone center, except at certain accidental band-crossing points [see Fig. 2(c)]. The spin texture near the Γ point [Fig. 2(d)] clearly demonstrates the Zeeman-type spin texture analogous to ferromagnets. The spin splitting is 99 meV and 66 meV for CBM and VBM at the Brillouin zone center, respectively. This rather large spin splitting is an order of magnitude larger than the maximum SOC-induced spin splitting in the whole Brillouin zone in $SrTiO_3/LaAlO_3$ heterostructures [53].

SST-4$_\alpha$ AFM compounds can be either polar or nonpolar. As shown in Fig. 2, $BiCrO_3$ is nonpolar. A polar example is Mn_2ScSbO_6, with its space group *R3* and magnetic space group *P1* (magnetic point group *1*). There are two nominal Wyckoff positions (*3a* and *3a*) for Mn in Mn_2ScSbO_6: one with all spin-up Mn^{2+} ions and the other with all spin-down Mn^{2+} ions. Thus, the Mn^{2+} ions are not connected by spin-interconverting auxiliary symmetries. We note that in Mn_2ScSbO_6, the nominal spin-down Mn^{2+} sites are partially substituted by Sc^{3+} (nonmagnetic), and the nominal Sc^{3+} sites (at Wyckoff position *3a* of the crystallographic space group *R3*) are partially substituted by spin-down Mn^{2+}. Considering the above cross substitutions, Mn_2ScSbO_6 still does not have any spin-interconverting auxiliary symmetry, and the total magnetization of Mn_2ScSbO_6 remains zero as the number of occupied spin-up and spin-down valence electrons are the same as the ideal structure [Fig. 3(a)] without cross substitutions, where the nominal spin-down *3a* Mn^{2+} sites are all occupied by spin-down Mn^{2+} and the nominal *3a* Sc^{3+} sites are all occupied by Sc^{3+}. Its MSG without SOC is *R3*, which does not have any spin-interconverting auxiliary symmetries. The compound was synthesized under high-pressure and high-temperature conditions with an antiferromagnetic order below $T_N = 22.3$ K [44].

Figure 3 shows our DFT results of the example polar α-type material Mn_2ScSbO_6 [see Fig. 3(a), space group: *R3*, magnetic space group: *P1*], which has a calculated, nearly direct insulating band gap of 1.96 eV. The CBM (Sc-*d* and O-p) and VBM (O-*p* and Mn-*d*) states have rather different orbital components [Fig. 3(b)], suggesting different spin-splitting properties [see, e.g., Fig. 3(c)]. The spin splitting is 158 meV and 160 meV for CBM and VBM at the Brillouin zone center, respectively. The spin splitting can appear throughout the whole Brillouin zone [see Figs. 3(c) and 3(d)]. In particular, Brillouin-zone-center spin splitting is found in Mn_2ScSbO_6 as all the spin-interconverting symmetries are broken. The calculated spin

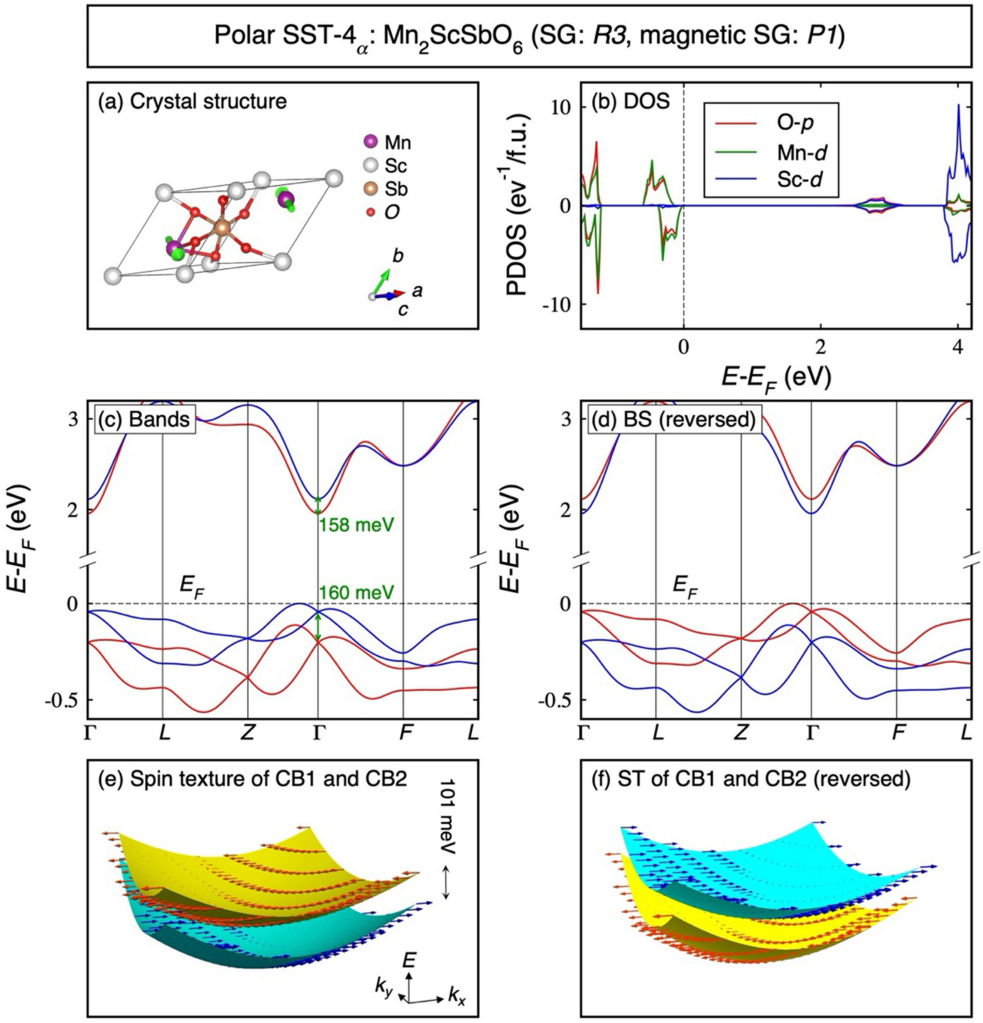

FIG. 3. Nonrelativistic (SOC = 0) spin splitting in polar α-type antiferromagnet Mn_2ScSbO_6 (space group: *R3*, magnetic space group: *P1*). (a) Crystal structure. The polar axis is along the z direction. (b) Partial density of states. (c) Band structure. Red (blue) curves in the band structure: spin-up (spin-down) polarized bands. The spin-splitting energies between the first two conduction bands and the first two valence bands at the Γ point, respectively, are indicated by green arrows. (d) Band structure of the reversed phase obtained by space-time reversal (ΘI). (e) Spin texture of the first and second conduction bands of the unreversed phase in the (001) plane around the Γ point. The magnetic moments and spin polarization are along the x axis. The range of $k_x(k_y)$ in the spin texture plot is $(-0.02, 0.02)\ 2\pi/\text{Å}$. (f) Spin texture of the first and second conduction bands of the reversed phase.

texture of Mn_2ScSbO_6 near the Brillouin zone center shows the strong spin polarization in the spin-split bands at the Γ point and Zeeman-type spin texture with spin vectors along the x axis.

The potential switching of NRSS along with polarity in Mn_2ScSbO_6 is demonstrated by comparing the electronic structures and spin textures of Mn_2ScSbO_6 and its reversed phase obtained by space-time reversal (ΘI), which have the same total energy as the original phase. We see that the reversed phase has an opposite nonrelativistic spin splitting from the original phase, suggesting the possibility to switch NRSS together with polarity. We further find that the spin texture is switched in the reversed phase as compared to the original phase [see Figs. 3(e) and 3(f)].

B. SST-4$_\beta$ subgroup: Rotational spin-interconverting auxiliary symmetry in polar or nonpolar systems

In β-type materials, the spin-sublattice interconverting auxiliary symmetry is the rotation symmetry with optional reflection symmetries. This subgroup has been dubbed "altermagnetism" [14], defined by its authors as having "opposite-spin sublattices connected by rotation (proper or improper and symmorphic or nonsymmorphic) but not connected by translation or inversion," although we do not assume that applying an auxiliary symmetry operation to AFM materials creates a new form of magnetism. Previously studied β-type materials are mostly nonpolar or even centrosymmetric [8,15,16,54–64], such as MnF_2 [8], MnTe [56,57,60–62], and RuO_2 [15,16,54,58,63,64].

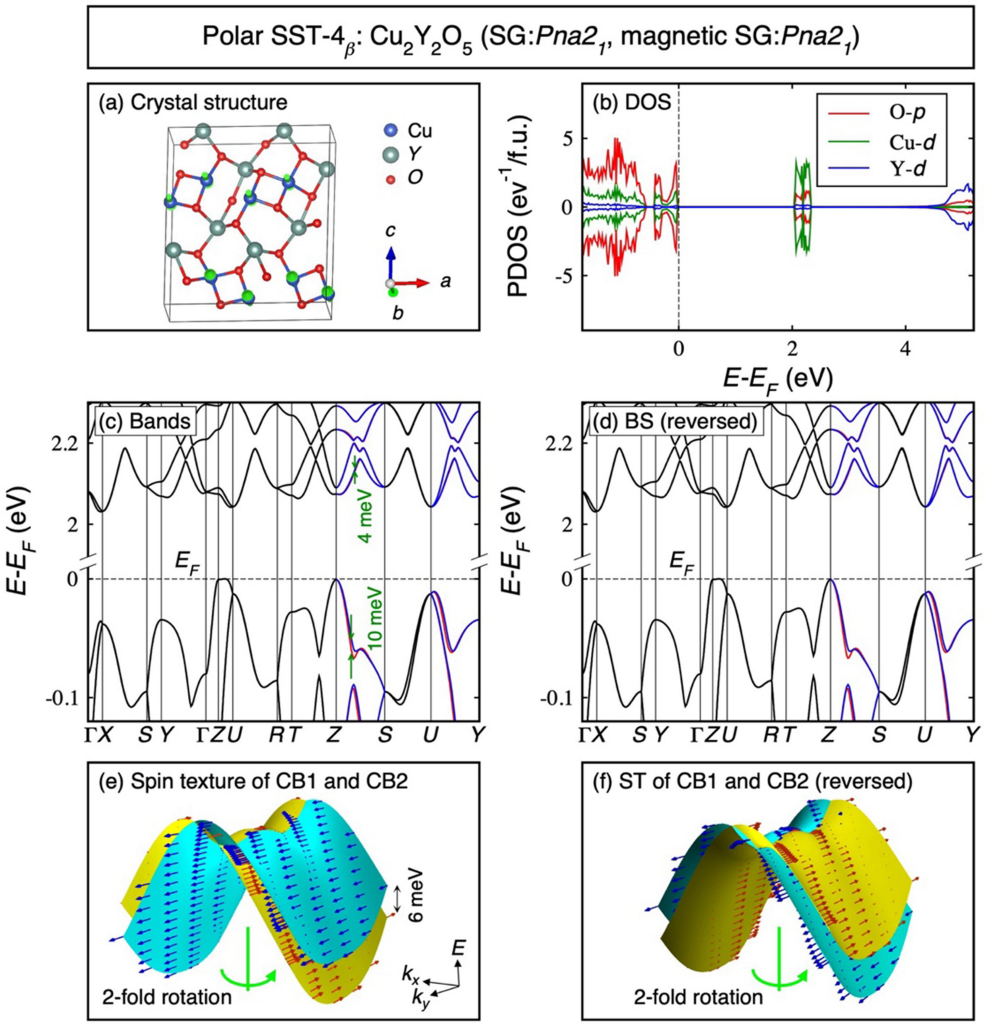

FIG. 4. Nonrelativistic (SOC = 0) spin splitting in polar β-type antiferromagnet $Cu_2Y_2O_5$ (space group: $Pna2_1$, magnetic space group: $Pna2_1$). (a) Crystal structure. The polar axis is along the z direction. (b) Partial density of states. (c) Band structure. Red (blue) curves in the band structure: spin-up (spin-down) polarized bands. Black curve: spin-degenerate bands. The largest spin-splitting energies between the first two conduction bands and the first two valence bands in panel (c), respectively, are indicated by green arrows. (d) Band structure of the reversed phase obtained by space-time reversal (ΘI). (e) Spin texture of the first and second conduction bands of the unreversed phase in the (001) plane around the $Z/2$ point. The magnetic moments and spin polarization are along the y axis. The range of $k_x(k_y)$ in the spin texture plot is $(-0.02, 0.02)$ $2\pi/\text{Å}$. (f) Spin texture of the first and second conduction bands of the reversed phase.

We identify a polar β-type compound $Cu_2Y_2O_5$ (space group: $Pna2_1$, magnetic space group: $Pna2_1$) with polar magnetic point group $mm2$ due to the existence of twofold rotation 2_z, which interconverts the opposite magnetic moments along the y direction. This compound was synthesized by a solid-state reaction showing an antiferromagnetic order with $T_N = 13$ K [45]. Polar β-type compounds offer a knob—polarity that may be reversed by an external electric field—to switch the alternating spin polarization electrically. For nonpolar materials, if the magnetic ordering is the knob that can be reversed (as in CuMnAs [65]), the spin polarization will be reversed simultaneously.

Figure 4 shows the DFT results of this compound, which has a band gap of 2.03 eV. The CBM (Cu-d) and VBM (O-p) states have rather different orbital components [Fig. 4(b)], suggesting diversified spin-splitting properties [see, e.g., Fig. 4(c)]. In this material, the local magnetic moments on the ions are compensated by each other due to the spin-interconverting rotation symmetry, leading to identical magnitudes of local magnetic moments on the spin-up and spin-down magnetic ions. The spin-interconverting rotation symmetry creates spin degeneracy at the Brillouin zone center [see Fig. 4(c)] and induces alternating spin polarization (spin texture) in the reciprocal space, with the spin polarization alternating plane perpendicular to the

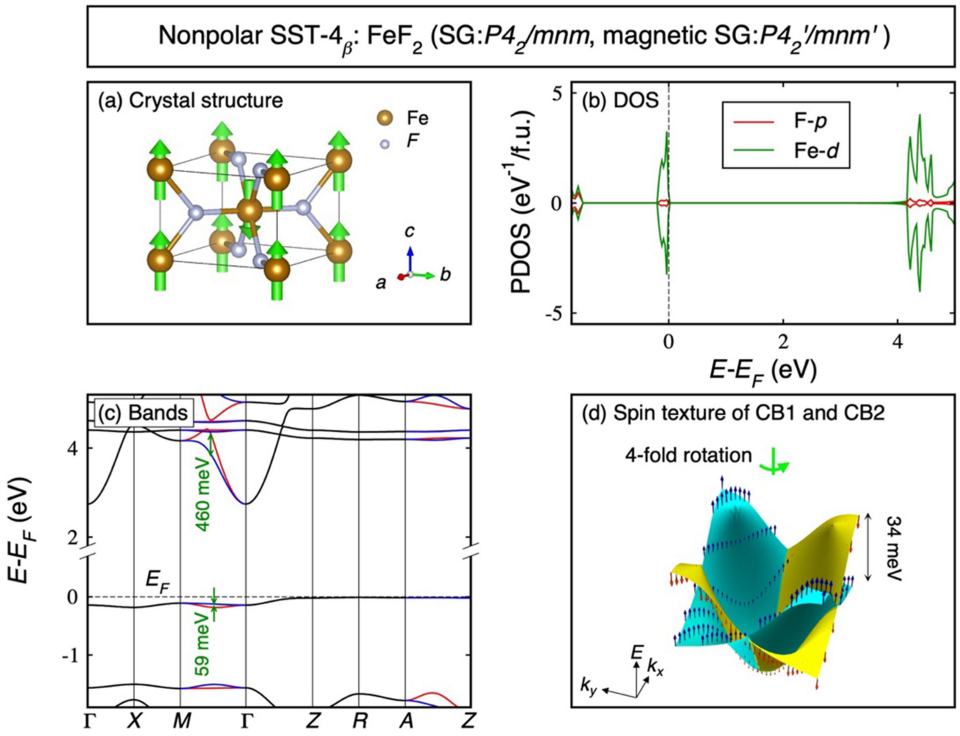

FIG. 5. Nonrelativistic (SOC = 0) spin splitting in nonpolar β-type antiferromagnet FeF_2 (space group: $P4_2/mnm$, magnetic space group: $P4_2'/mnm'$). (a) Crystal structure. (b) Partial density of states. (c) Band structure. Red (blue) curves in the band structure: spin-up (spin-down) polarized bands. Black curve: spin-degenerate bands. The largest spin-splitting energies between the first two conduction bands and the first two valence bands in panel (c), respectively, are indicated by green arrows. (d) Spin texture of the first and second conduction bands in the (001) plane around the $Z/2$ point. The magnetic moments and spin polarization are along the z axis. The range of $k_x(k_y)$ in the spin texture plot is $(-0.02, 0.02)$ $2\pi/\text{Å}$.

polar axis [see Fig. 4(e)]. The switching of NRSS along with polarity in $Cu_2Y_2O_5$ is demonstrated by comparing the electronic structures and spin textures of $Cu_2Y_2O_5$ and its reversed phase obtained by spatial inversion and reversal of all magnetic moments (with the same total energy as the original phase). We see that the reversed phase has opposite spin splitting from the original phase, suggesting the possibility of switching spin splitting together with polarity. The spin texture is switched in the reversed phase of $Cu_2Y_2O_5$ as compared to the original phase [see Figs. 4(e) and 4(f)]. The twofold symmetric spin texture in $Cu_2Y_2O_5$ [Figs. 4(e) and 4(f)] is induced by the two-fold screw axis 2_1 as well as the glide reflection n discussed above that maps spin-up ions to spin-down ions.

In Fig. 5, we also show the DFT results of FeF_2 as an example of nonpolar SST-4$_\beta$ AFM compounds. The compound FeF_2 has the crystallographic space group $P4_2/mnm$ and magnetic space group $P4_2'/mnm'$ (magnetic point group $4'/mm'm$) [47]. The fourfold rotation with time-reversal symmetry $4_z'$ interconverts the opposite magnetic moments along the z direction. It was grown from the melt, possessing the rutile structure [46]. It is found that FeF_2 orders antiferromagnetically at 78 K, with the opposing moments aligned along the c axis of the tetragonal crystal [47]. FeF_2 has the same symmetry as the first predicted β-type material MnF_2 [8], and it also possesses fourfold alternating spin polarizations (see Fig. 5). As FeF_2 was not found in the MAGNDATA database [35], we use the magnetic configuration of MnF_2 [8].

C. SST-4$_\gamma$ subgroup: Exclusively reflection spin-interconverting auxiliary symmetry in polar only systems

In γ-type materials, the spin-sublattice interconverting auxiliary symmetry is the exclusive reflection symmetry. An example material is $Mn_4Nb_2O_9$, which was synthesized by a solid-state reaction [48,66], with AFM below $T_N = 109.1$ K showing magnetoelectric properties [48]. $Mn_4Nb_2O_9$ is polar with crystallographic space group Cc and magnetic space group Cc (magnetic point group m). In γ-type materials, the polarity may be reversed by an external electric field, offering a knob to switch the spin polarization electrically.

The only spin-interconverting auxiliary symmetry found in $Mn_4Nb_2O_9$ is the glide reflection symmetry m_y that interconverts the opposite magnetic moments along the z direction. Figure 6 shows our DFT results of $Mn_4Nb_2O_9$, which has a band gap of 2.39 eV. The CBM (Nb-d) and VBM (Mn-d and O-p) states have rather different orbital components [Fig. 6(b)], suggesting different spin-splitting

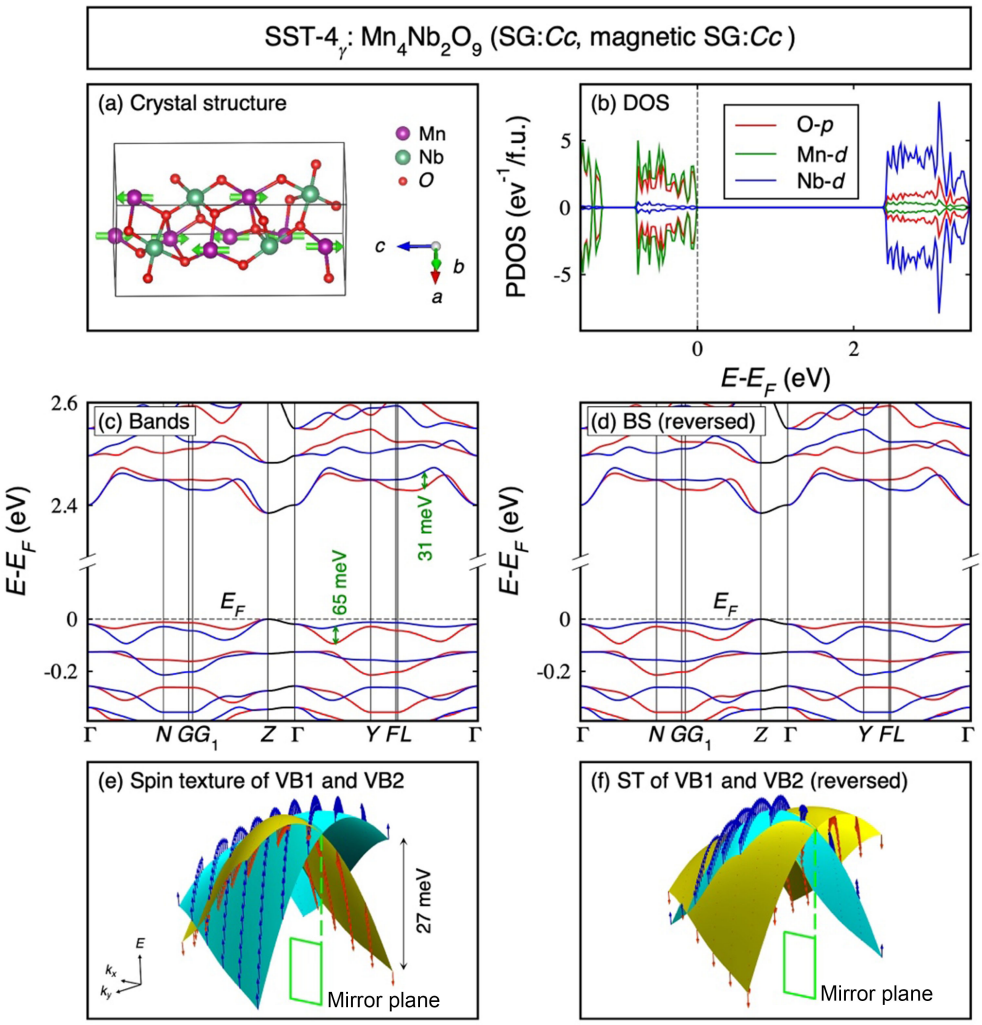

FIG. 6. Nonrelativistic (SOC = 0) spin splitting in (polar) γ-type antiferromagnet exclusively reflection symmetry without rotation symmetry, $Mn_4Nb_2O_9$ (space group: *Cc*, magnetic space group: *Cc*). (a) Crystal structure. The polar axis is along the z direction. (b) Partial density of states. (c) Band structure. Red (blue) curves in the band structure: spin-up (spin-down) polarized bands. Black curve: spin-degenerate bands. The largest spin-splitting energies between the first two conduction bands and the first two valence bands in panel (c), respectively, are indicated by green arrows. (d) Band structure of the reversed phase obtained by space-time reversal (ΘI). (e) Spin texture of the first and second valence bands of the unreversed phase in the k plane perpendicular to the magnetic moment around the $Z/2$ point, where the magnetic moments and spin polarization are perpendicular to the *ab* plane of the monoclinic unit cell. The range of $k_x(k_y)$ in the spin texture plot is $(-0.02, 0.02)$ $2\pi/\text{Å}$. (f) Spin texture of the first and second valence bands of the reversed phase.

properties. In this material, the local magnetic moments on the ions are mutually compensated due to the spin-mapping reflection symmetry, leading to zero total magnetization. The spin-interconverting reflection auxiliary symmetry creates spin degeneracy at the Brillouin zone center but allows spin splitting along most of the k lines except Z-Γ, where the spin degeneracy is protected by the auxiliary symmetry [see Figs. 6(c) and 6(d)]. The spin degeneracy along Z-Γ is protected by the spin-interconverting glide reflection symmetry. Notably, the spin texture is symmetric with respect to the mirror plane as indicated in Figs. 6(e) and 6(f). The k regions with opposite spin polarization [see Figs. 6(e) and 6(f)] in the spin texture are connected by the glide reflection symmetry c of the MSG. This spin texture shaped by the auxiliary reflection symmetry is different from the "alternating" spin texture in β-type materials. Figures 6(e) and 6(f) also compare the electronic structures of $Mn_4Nb_2O_9$ and its reversed phase obtained by space-time reversal (ΘI), demonstrating the switching of spin splitting along with polarity. The reversed phase has an opposite spin-polarized splitting from the original phase, and the spin texture is switched in the reversed phase.

Another example of γ-type materials is $FeScO_3$, which was synthesized by conventional solid-state methods [49]. Neutron powder diffraction shows that $FeScO_3$ is

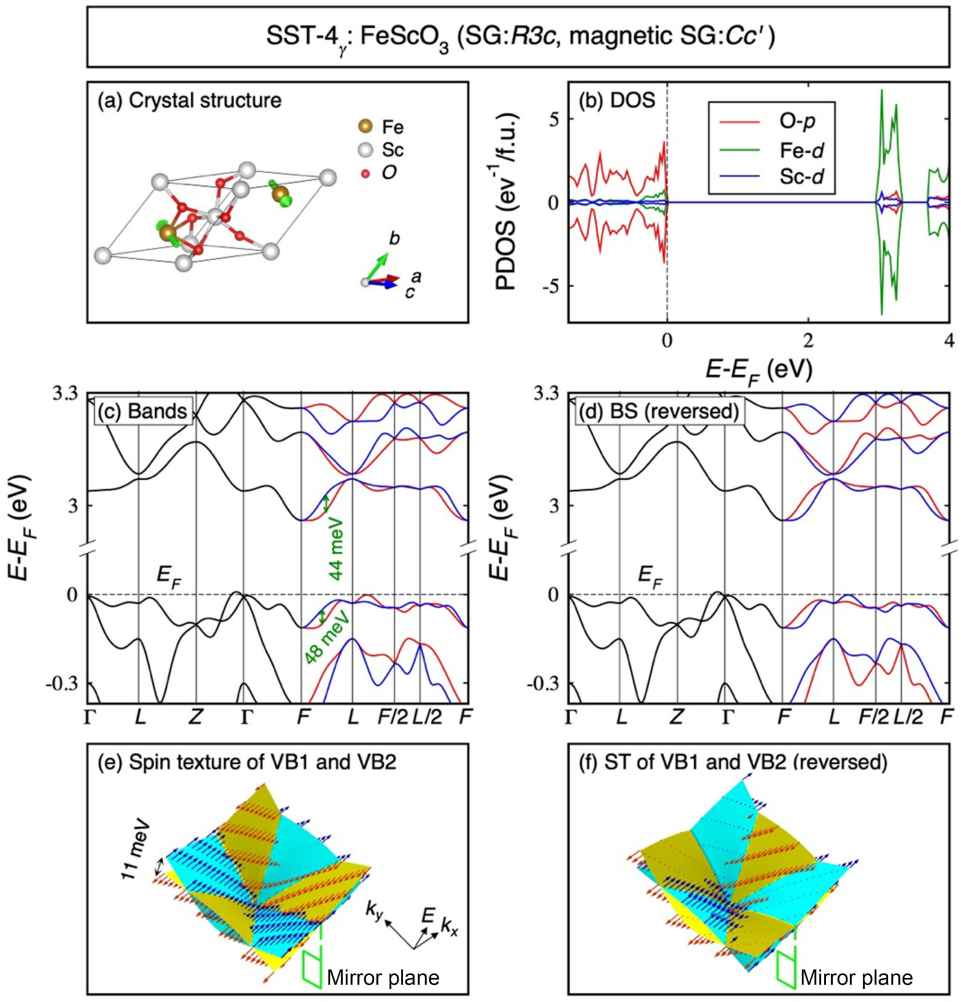

FIG. 7. Nonrelativistic (SOC = 0) spin splitting in γ-type antiferromagnet $FeScO_3$ (space group: $R3c$, magnetic space group: Cc'). (a) Crystal structure. The polar axis is along the z direction. (b) Partial density of states. (c) Band structure. Red (blue) curves in the band structure: spin-up (spin-down) polarized bands. Black curve: spin-degenerate bands. The largest spin-splitting energies between the first two conduction bands and the first two valence bands in panel (c), respectively, are indicated by green arrows. (d) Band structure of the reversed phase obtained by space-time reversal (ΘI). (e) Spin texture of the first and second valence bands of the unreversed phase in the (001) plane around the $Z/2$ point. The magnetic moments and spin polarization are along the x axis. The range of $k_x(k_y)$ in the spin texture plot is $(-0.02, 0.02)$ $2\pi/\text{Å}$. (f) Spin texture of the first and second valence bands of the reversed phase.

magnetically ordered at 300 K, adopting an antiferromagnetic structure with antiparallel spins for all nearest neighbors [49]. $FeScO_3$ is polar with crystallographic space group $R3c$ and magnetic space group Cc' (magnetic point group m').

The spin-interconverting auxiliary symmetry in $FeScO_3$ is the glide reflection symmetry m'_y that interconverts the opposite magnetic moments along the y direction. Figure 7 shows the DFT results of $FeScO_3$, which has a band gap of 2.96 eV. The VBM (CBM) states consist mainly of O-p (Fe-d) states [Fig. 7(b)]. In $FeScO_3$, the local magnetic moments on the ions are mutually compensated due to the spin-interconverting reflection symmetry, leading to zero total magnetization. In this material, the Fe^{3+} sites are partially substituted by Sc^{3+} (nonmagnetic), and the Sc^{3+} sites are partially substituted by Fe^{3+}. In the average (virtual) crystal approach used to analyze such cross-substituted systems, $FeScO_3$ is assumed to have the spin-interconverting glide reflection symmetry with magnetic space group Cc' as in the ideal structure [Fig. 7(a)] without cross substitutions, where the nominal $6a Fe^{3+}$ sites are all occupied by Fe^{3+} and the nominal $6a Sc^{3+}$ sites are all occupied by Sc^{3+}. Such spin-interconverting reflection symmetry creates spin degeneracy at the Brillouin zone center but allows spin splitting to appear along some low-symmetric k lines [see Figs. 7(c) and 7(d)].

The symmetry analysis of the spin texture in $FeScO_3$ is related to the different approaches discussed in Sec. III: Approach (i) MSG without SOC [40] assumes that the direction of local magnetic moments has no impact on the magnetic symmetry and physical properties. In this case,

the glide reflection symmetry m'_y of the MSG without SOC ($R3c'$) of $FeScO_3$ suggests three mirror planes parallel to the z axis, including the (100) plane. In the more general approach (ii), MSG [8] includes the direction of local magnetic moments that could have an impact on magnetic symmetry and physical properties (e.g., directions of total magnetizations in SST-4_α compounds at nonzero temperatures). In this case, the glide reflection symmetry m'_y of the MSG suggests one mirror plane, i.e., the (100) plane, as shown in Figs. 7(e) and 7(f) for both the unreversed and reversed phases. Significantly, both approaches (i) and (ii) reveal the reflection auxiliary symmetry in this γ-type material. In the DFT calculations [see Figs. 7(e) and 7(f)], the spin texture is indeed found to be symmetric with respect to the (100) mirror plane, meaning the result is consistent with approach (ii) with a single mirror plane.

D. Differences between SST-4_β and SST-4_γ subgroups

In the present paper, we define SST-4_β as having auxiliary rotation (with optional reflection), but SST-4_γ is defined as having exclusively reflection. This finding leads to experimentally detectable differences in both crystal symmetry and spin textures. Note that, as is the case with all SST definitions, it defines the magnetocrystallographic symmetry of physical crystal not the specific symmetry of individual wave functions $\psi(n,k)$, as is the case in spin Laue group qualifications. First, one can distinguish β-type from γ-type materials by the auxiliary symmetries: The spin-interconverting auxiliary symmetry in γ-type materials is exclusively reflection symmetry without any rotation symmetry, while that in β-type materials is rotation symmetry with optional reflection symmetry. Second, the ensuing properties of β-type and γ-type materials are predicted to be different: The γ-type crystal can only be polar, while the β-type materials can be either polar or nonpolar. This clear difference in the crystalline potential of the two subgroups drives subsequent differences. Regarding the spin texture, the γ-type materials have mirror-reflectional spin-polarized bands in reflection-connected k-point regions, while the β-type materials have "alternating" spin-polarized bands in rotation-connected k-point regions. The spin degeneracy is protected by different spin-interconverting symmetries—reflection in γ-type materials [such as the (010) plane and (100) plane in $Mn_4Nb_2O_9$ and $FeScO_3$ as shown in Figs. 6(e) and 7(e), respectively] and rotation in β-type materials [such as the C_{2z} axis and C_{4z} axis in $Cu_2Y_2O_5$ and FeF_2 as shown in Figs. 4(e) and 5(c), respectively].

E. Selection of SST-4 subgroups using magnetic point groups without spin-orbit coupling

As we introduced in Sec. III, we use the MPG that contains (i) the crystallographic space group, (ii) the lattice direction of magnetic moments, and (iii) explicit allowance of SOC. These ingredients are sufficient and fully consistent with the DFT method we use throughout the paper to describe real collinear magnetic materials with or without SOC. On the other hand, MPG without SOC, as well as the spin point group, decouples the spin and space degrees of freedom, hence making the lattice direction of magnetic moments have no impact on the magnetic symmetry in collinear magnetic systems. In this section, we briefly discuss the MPG without SOC (i.e., without including explicitly lattice orientation of the magnetic moments) for classifying the three spin-interconverting subgroups α, β, and γ. For simplicity, we use MPG to refer to MPG without SOC below in this section.

For the α subgroup, the MPGs require the absence of time-reversal symmetry, making the opposite magnetic moments not interconverted by any symmetry. Even when rotation or reflection operations (without time-reversal symmetry) exist in certain MPGs, these operations cannot interconvert opposite moments, thus leading to α-type behavior, for example, operations 2_y and m_y in MPG $2/m$ (such as $BiCrO_3$) and operation 3_z in MPG 3 (such as Mn_2ScSbO_6).

For β and γ subgroups, the MPGs require the existence of time-reversal symmetry. The β subgroup requires the combination of rotation and time-reversal symmetry, such as operation $2'_z$ in MPG $m'm2'$ (such as $Cu_2Y_2O_5$) and operation $4'_z$ in MPG $4'/mm'm$ (FeF_2). The γ subgroup exclusively requires the combination of mirror reflection and time-reversal symmetry, such as operation m'_y in MPG m' (such as $Mn_4Nb_2O_9$) and operation m'_y in MPG $3m'$ (such as $FeScO_3$). Most collinear SST-4 MPGs belong to the β subgroup, such as $4'/mm'm$, $2'/m'$, $2'2'2$, etc. For the γ subgroup, we find five MPGs: m', $m'm'2$, $4m'm'$, $3m'$, and $6m'm'$.

V. FULLY COMPENSATED, QUASI-COMPENSATED, AND UNCOMPENSATED SST-4 SUBGROUPS

In this section, we discuss the behavior of magnetization of SST-4 subgroups under perturbations. Different materials with different structures, and electronic, phononic, or magnetic properties are likely to be responsive in different ways to perturbations in the net magnetization. It is not our purpose to specify different mechanisms for different materials but instead to use a generic model that characterizes such perturbations by a model of effective broadening of the Fermi-Dirac distribution that can be treated on the DFT level. This Fermi smearing method is simple but captures the core features of temperature influences in the magnetization, as shown in Fig. 8. Therefore, to understand the $M(T)$ behavior and drive a clear distinction, we use the DFT calculated band structures and self-consistent spin densities to model $M(T)$ for α-, β-, and γ-type compounds and compensated ferrimagnets. Recall that the total magnetic moment of the crystal consists of the sum of ionic local magnetic moments plus the magnetic moments associated with the spin of the electrons that are not bound

to ions. In particular, the ionic local magnetic moments alone do not have to sum over atomic sites to zero [40] since they can be compensated by the electrons that are not bounded to ions. Here, we use the "Fermi smearing method" [67] in the electronic-state calculations via introducing an effective electronic temperature in the physical canonical ensemble of the electronic system based on the Fermi-Dirac function, where the smearing magnitude ($\sigma = k_B T$) corresponds to the effective temperature (T) of the electronic system; i.e., the occupation function of the electronic states is modeled by the Fermi-Dirac distribution:

$$\bar{N}(\varepsilon) = \frac{g(\varepsilon)}{e^{(\varepsilon-\mu)/\sigma}+1}, \tag{1}$$

where k_B is the Boltzmann constant, $g(\varepsilon)$ is the density of states at energy level ε, and μ is the Fermi level.

The results for the total magnetization as a function of effective temperature are shown in Fig. 8 for two α-type AFM materials ($BiCrO_3$ and Mn_2SbScO_6), a β-type AFM material (FeF_2), and a γ-type AFM ($FeScO_3$), as well as for a compensated ferrimagnet ($CrFeS_2$). We find the following: (i) At zero temperature, all these materials have zero total magnetization; (ii) at finite effective temperatures, the total magnetization of α-type AFM materials is nonzero but exceedingly tiny, practically antiferromagnetic-like at all physically relevant temperatures below T_N (e.g., 0.0003 μ_B at 2000 K in Mn_2ScSbO_6); (iii) the total magnetization of the α-type AFM ($BiCrO_3$ and Mn_2ScSbO_6) is very different from the compensated ferrimagnets ($CrFeS_2$), as the latter have relatively large nonzero values at finite temperatures and increase rapidly (e.g., 0.0299 μ_B at 2000 K).

The α-type materials are distinguished by a symmetry rule as well as by chemical circumstances that enable low net magnetization even under thermal and other perturbations. Symmetry-wise, α-type NRSS is free from spin-interconverting symmetry that forces mapping of one spin into another, unlike the case in β- and γ-type materials. The chemical condition that provides α-type AFM zero magnetization at zero temperature and weak magnetization under perturbed filling conditions is the presence of a single, unique, magnetic ion type, which is illustrated by the examples given in Fig. 8. The distinction between α-type AFM materials and compensated ferrimagnets is that α-type materials, just like compensated ferrimagnets, have zero magnetization at zero temperature $[M(T=0)=0]$; however, α-type materials can have (see Fig. 8) considerably smaller magnetization under external perturbations such as finite temperatures. In contrast, uncompensated ferrimagnets have $M(T=0)>0$ and $M(T>0)>0$. The compositional difference between α-type AFM materials

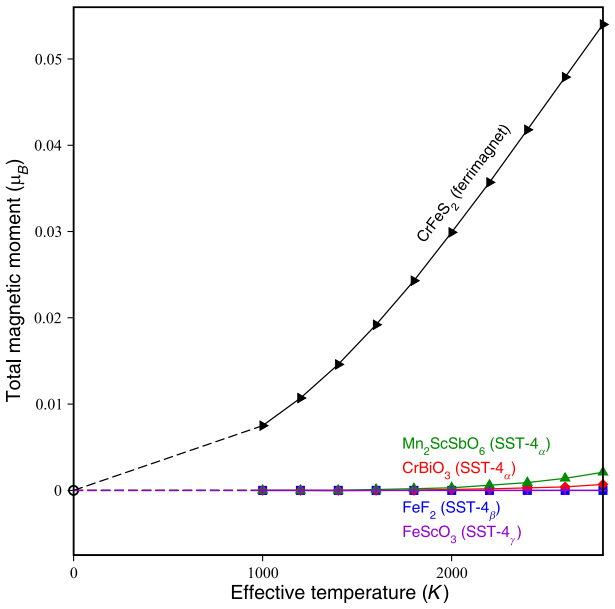

FIG. 8. Total magnetic moments as functions of effective temperature in Fermi smearing that represent the temperature in the electronic system for different magnets having zero total magnetization at zero temperature.

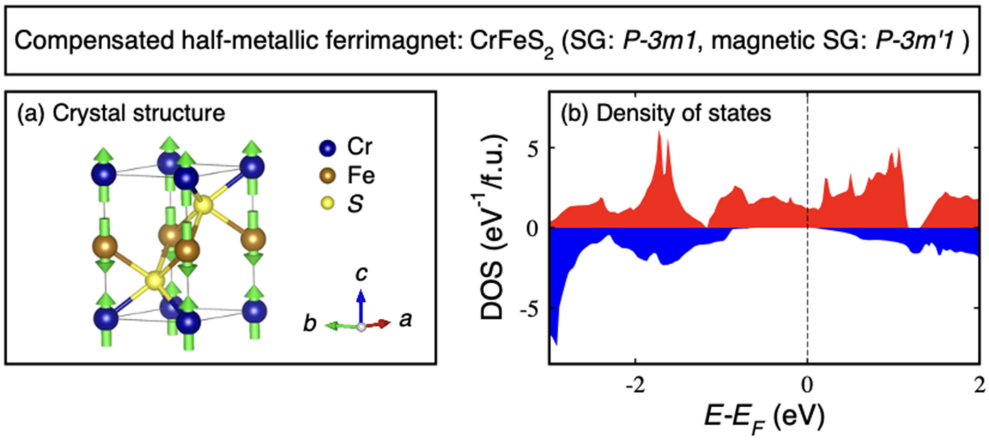

FIG. 9. (a) Crystal structure and (b) spin-polarized density of states of compensated half-metallic ferrimagnet $CrFeS_2$.

and compensated ferrimagnets is that chemical identities of the two opposite-spin ions are the same in the former but different in the latter.

Rather obviously, two mechanisms are involved [51,52]: "symmetry-enforced null magnetization" (e.g., β-type auxiliary symmetries forcing null magnetization at all temperatures in FeF_2; see Fig. 8) and "orbital filling-enforced total magnetization," which reflects thermal excitation across the band gap. The latter factor depends on the band gap. The two α-type AFM compounds have rather large DFT band gaps (1.69 eV and 1.96 eV for $BiCrO_3$ and Mn_2ScSbO_6, respectively), leading to the tiny net magnetization even at high temperatures (Fig. 8). Conceivably, low gap compounds or even metals will have high magnetization unless there are spin-interconverting symmetries. The compensated ferrimagnetic materials shown happen to have two different magnetic ions that contribute, together with the electron zero magnetization at $T = 0$; however, on account of being half metallic (the gap is insulating for one spin direction and metallic for the other; see Fig. 9), the magnetization rises rapidly at finite T. Thus, for α-type AFM materials that are highly insulating with a unique, single magnetic ion ($BiCrO_3$ and Mn_2ScSbO_6), they are clearly distinct from $T = 0$ compensated ferrimagnets with different magnetic ions, such as $CrFeS_2$.

VI. DISCUSSION

A. Effect of spin-orbit coupling on the spin splitting in different subgroups of SST-4 materials

In summary, the classification of subgroups is done by allowing spin and space coupling [approach (ii) including SOC], as shown in Table III. All the band structures in Figs. 2–7 are performed without SOC in the Hamiltonian. Table IV examines the possible difference in band structure, showing rather small differences, for all subgroups.

In this paper, we mainly focus on the spin splitting and spin textures of different subgroups of NRSS materials originating from magnetism, instead of SOC, i.e., NRSS. SOC can induce spin splitting in noncentrosymmetric nonmagnetic materials away from the Brillouin zone center [4,6]. The SOC-induced spin splitting could numerically affect the NRSS shown in Figs. 2–7. As an example, we consider a polar β-type NRSS system with fourfold alternating spin polarization as shown in Fig. 1, which can be represented by the following single-band Hamiltonian:

$$H_0 = \frac{1}{2m^*}(k_x^2 + k_y^2 + k_z^2) + \mathrm{A}_1 k_x k_y \sigma_z, \tag{2}$$

where m^* is the effective mass, A_1 is the coefficient representing the strength of the nonrelativistic spin splitting, k_i are the components of the momentum, and σ_z is a Pauli matrix. The crystal's polarity will induce Rashba spin splitting and add an additional term in the Hamiltonian:

$$H_0 = \frac{1}{2m^*}(k_x^2 + k_y^2 + k_z^2) + \mathrm{A}_1 k_x k_y \sigma_z + \mathrm{A}_2(k_x\sigma_y - k_y\sigma_x), \tag{3}$$

where A_2 is the coefficient representing the strength of the Rashba spin splitting. In this scenario, the SOC-induced spin splitting, here the Rashba spin splitting, will further split the spin bands that are already split by the NRSS effect.

In reality, SOC could slightly change the magnetism and magnitude of magnetic moments, induce coupling between different bands, and change the relationship between magnetic ions, thus inducing spin-splitting effects in AFM materials beyond the single-band assumption. Table IV compares the spin splitting with and without SOC for the same set of k points of the calculated NRSS materials (see Figs. 2–7), with the crystal structures relaxed by DFT. The relative variation with and without SOC spreads from less than 1% to 48%. The SOC effect is taken into account by a perturbation $\sum_{i,l,m} V_l^{SO}\mathbf{L}\cdot\mathbf{S}|l,m\rangle_{ii}\langle l,m|$ to the pseudopotential, where $|l,m\rangle_i$ is the angular-momentum eigenstate of the ith atomic site [68]. For α-type

TABLE IV. Nonrelativistic spin-splitting energies between the lowest two conduction bands (highest two valence bands) of the example α-type materials at the Γ point and the β-type and γ-type materials at specific k points (indicated by green arrows in Figs. 4–7), where the calculated lowest two conduction bands (highest two valence bands) have the largest nonrelativistic spin splitting, as well as the corresponding spin splitting with spin-orbit coupling at the same k points with the crystal structures relaxed by PBE + U.

Material	$\Delta E_{\mathrm{SS-CB}}^{\mathrm{no-SOC}}(k_{\mathrm{CB}})$ (meV)	$\Delta E_{\mathrm{SS-CB}}^{+\mathrm{SOC}}(k_{\mathrm{CB}})$ (meV)	$\Delta E_{\mathrm{SS-VB}}^{\mathrm{no-SOC}}(k_{\mathrm{VB}})$ (meV)	$\Delta E_{\mathrm{SS-VB}}^{+\mathrm{SOC}}(k_{\mathrm{VB}})$ (meV)
$BiCrO_3$ (nonpolar α type, Fig. 2)	99	104	66	72
Mn_2ScSbO_6 (polar α type, Fig. 3)	158	158	160	161
$Cu_2Y_2O_5$ (polar β type, Fig. 4)	4	5	10	10
FeF_2 (nonpolar β type, Fig. 5)	460	457	59	59
$Mn_4Nb_2O_9$ (γ type, Fig. 6)	31	46	65	65
$FeScO_3$ (γ type, Fig. 7)	44	52	48	51

materials, we choose the Γ point to represent the unique Brillouin-zone-center spin splitting. For β-type and γ-type materials, we choose the k points where the lowest two calculated conduction bands (highest two valence bands) have the largest NRSS. We find the following: (i) In most cases, SOC has an negligible effect on spin splitting except for the conduction bands of $Mn_4Nb_2O_9$, where a significant increase of spin splitting by SOC is found (because $Mn_4Nb_2O_9$ is polar and its conduction band states are mainly formed by the d states of relatively heavy Nb); (ii) a nonnegligible increase of spin splitting due to SOC is found even in centrosymmetric compounds such as $BiCrO_3$ and even at the Γ point.

B. Potential for application of NRSS prototypes in spintronics

The prototypes of NRSS materials (α-type, β-type, and γ-type) discussed in this study can significantly enrich the materials space of NRSS for their application in next-generation spintronic devices. The breaking of time-reversal symmetry [14,69] and spin splitting of these prototypes of NRSS materials can lead to nonzero spin conductivities, as shown for the β-type materials in Ref. [70]. As the anomalous Hall effect is studied in β-type materials [71], we offer a very different prototype (α-type) that possesses electronic structures analogous to ferromagnets but have zero (almost zero) total magnetic moments at zero (finite) temperature, which could potentially possess anomalous Hall effects beyond ferromagnets. Moreover, the α-type materials can have either insulating or half-metallic band structure, which guarantees the presence of spin-polarized free carriers while keeping the AFM spin configuration, likely providing potential new spin transporting applications. As the exchange-driven spin Hall effect was recently predicted in the ferromagnetic materials with anisotropic conductivity tensors [72], it may also be interesting to search for α-type AFM with anisotropic conductivity tensors for the possibility to realize such an effect in AFM. Furthermore, the unique spin textures of insulating β-type and γ-type compounds can induce special spin filtering properties in the insulating barrier layers of the spin filter devices as demonstrated in β-type insulators MF_2 (M = Fe, Co, Ni) [73,74]. The metallic β-type and γ-type compounds could also offer spin splitting or spin textures for the spin-split electrode layers of the spin filter or tunneling magnetoresistance spintronic devices, as demonstrated for β-type metal RuO_2 [15]. The electric polarization in polar α-type and β-type as well as γ-type materials offers the opportunity to switch the magnetic configuration and spin texture via electrical means, enabling the electrically operated, non-stray-field and potentially high-frequency spintronic devices. Recent works [34,75,76] on switching spin-splitting AFM materials with a cofunctionality of ferroelectricity or antiferroelectricity are closely related to the polarity in these materials. Our current work will provide the symmetry guidance for future electric-switchable AFM candidates with NRSS. Furthermore, some new classifications of magnets were recently proposed [32] to try to connect the NRSS AFM to other physical effects. Cofunctionality X with NRSS in AFM materials will be an interesting project in this field, though it is not necessary for NRSS AFM to spontaneously have the functionality X (e.g., X = topological electronic structures [77], anomalous Hall effects [78], etc.). Analogous to the high-order rotational symmetries (e.g., C_3 or C_4) in nonmagnets that can protect Dirac band crossings forming Dirac semimetal phases [79,80], the high-order spin-interconverting rotational symmetries in β-type antiferromagnets can protect Dirac points on the rotation axes to form magnetic Dirac semimetals. Such high-order spin-interconverting rotational symmetries are absent in γ-type systems. Last but not least, for the example NRSS materials with band gaps (1.69–2.96 eV) in the visible light regime suitable for optoelectronic applications (see Figs. 2–7), the spin splitting can be controlled optically by changing the occupation of the electronic levels during the photoexcitation process, as demonstrated for a theoretical model of a β-type NRSS system [81].

ACKNOWLEDGMENTS

The formal theory of symmetry subgroups was supported by the National Science Foundation (NSF) DMR-CMMT Grant No. DMR-2113922. The DFT calculations of electronic and magnetic properties were supported by the U.S. Department of Energy, Office of Science, Basic Energy Sciences, Materials Sciences and Engineering Division under Grant No. DE-SC0010467. This work used resources of the National Energy Research Scientific Computing Center, which is supported by the Office of Science of the U.S. Department of Energy. This work also used resources of the Stampede3 system at Texas Advanced Computing Center through allocation PHY180030 from the Advanced Cyberinfrastructure Coordination Ecosystem: Services & Support (ACCESS) program, which is supported by National Science Foundation Grants No. 2138259, No. 2138286, No. 2138307, No. 2137603, and No. 2138296.

DATA AVAILABILITY

The data that support the findings of this article are not publicly available. The data are available from the authors upon reasonable request.

[1] H. A. Jahn and E. Teller, *Stability of polyatomic molecules in degenerate electronic states I-orbital degeneracy*, Proc. R. Soc. A **161**, 220 (1937).

[2] J. B. Goodenough, *Direct cation–cation interactions in several oxides*, Phys. Rev. **117**, 1442 (1960).

[3] O. I. Malyi and A. Zunger, *False metals, real insulators, and degenerate gapped metals*, Appl. Phys. Rev. **7**, 041310 (2020).

[4] E. I. Rashba, *Properties of semiconductors with an extremum loop. 1. Cyclotron and combinational resonance in a magnetic field perpendicular to the plane of the loop*, Sov. Phys.-Solid State **2**, 1109 (1960).

[5] Y. A. Bychkov and E. I. Rashba, *Properties of a 2D electron-gas with lifted spectral degeneracy*, JETP Lett. **39**, 78 (1984).

[6] G. Dresselhaus, *Spin-orbit coupling effects in zinc blende structures*, Phys. Rev. **100**, 580 (1955).

[7] S. I. Pekar and E. I. Rashba, *Combined resonance in crystals in inhomogeneous magnetic fields*, Zh. Eksp. Teor. Fiz. **47**, 1927 (1964).

[8] L. D. Yuan, Z. Wang, J. W. Luo, E. I. Rashba, and A. Zunger, *Giant momentum-dependent spin splitting in centrosymmetric low-Z antiferromagnets*, Phys. Rev. B **102**, 014422 (2020).

[9] M. Naka, S. Hayami, H. Kusunose, Y. Yanagi, Y. Motome, and H. Seo, *Spin current generation in organic antiferromagnets*, Nat. Commun. **10**, 4305 (2019).

[10] S. Hayami, Y. Yanagi, and H. Kusunose, *Momentum-dependent spin splitting by collinear antiferromagnetic ordering*, J. Phys. Soc. Jpn. **88**, 123702 (2019).

[11] K. H. Ahn, A. Hariki, K. W. Lee, and J. Kunes, *Antiferromagnetism in* RuO_2 *as d-wave Pomeranchuk instability*, Phys. Rev. B **99**, 184432 (2019).

[12] H. Y. Ma, M. L. Hu, N. N. Li, J. P. Liu, W. Yao, J. F. Jia, and J. W. Liu, *Multifunctional antiferromagnetic materials with giant piezomagnetism and noncollinear spin current*, Nat. Commun. **12**, 2846 (2021).

[13] I. I. Mazin, K. Koepernik, M. D. Johannes, R. González-Hernández, and L. Smejkal, *Prediction of unconventional magnetism in doped* $FeSb_2$, Proc. Natl. Acad. Sci. U.S.A. **118**, e2108924118 (2021).

[14] L. Smejkal, J. Sinova, and T. Jungwirth, *Beyond conventional ferromagnetism and antiferromagnetism: A phase with nonrelativistic spin and crystal rotation symmetry*, Phys. Rev. X **12**, 031042 (2022).

[15] L. Smejkal, A. B. Hellenes, R. González-Hernández, J. Sinova, and T. Jungwirth, *Giant and tunneling magnetoresistance in unconventional collinear antiferromagnets with nonrelativistic-momentum*, Phys. Rev. X **12**, 011028 (2022).

[16] L. Smejkal *et al.*, *Chiral magnons in altermagnetic* RuO_2, Phys. Rev. Lett. **131**, 256703 (2023).

[17] I. V. Solovyev, *Magneto-optical effect in the weak ferromagnets* $LaMO_3$ *(*M = Cr*, Mn, and Fe)*, Phys. Rev. B **55**, 8060 (1997).

[18] S. López-Moreno, A. H. Romero, J. Mejía-López, A. Muñoz, and I. V. Roshchin, *First-principles study of electronic, vibrational, elastic, and magnetic properties of* FeF_2 *as a function of pressure*, Phys. Rev. B **85**, 134110 (2012).

[19] M. Kissel-Phillip and W. H. E. Schwarz, *Relativistically corrected Schrodinger-equation*, Phys. Rev. A **38**, 6027 (1988).

[20] L. Pauling, *The nature of the chemical bond IV The energy of single bonds and the relative electronegativity of atoms*, J. Am. Chem. Soc. **54**, 3570 (1932).

[21] S. H. Wei and A. Zunger, *Electronic-structure of II-VI compounds and their alloys—role of cation d-bands*, J. Cryst. Growth **86**, 1 (1988).

[22] D. J. Friedman, G. P. Carey, I. Lindau, and W. E. Spicer, *Effect of different cation-anion bond strengths on metal ternary-semiconductor interface formation—*$Cu/Hg_{0.75}Cd_{0.25}Te$ *and* Cu/CdTe, Phys. Rev. B **34**, 5329 (1986).

[23] B. Weber, Y. L. Hsueh, T. F. Watson, R. Y. Li, A. R. Hamilton, L. C. L. Hollenberg, R. Rahman, and M. Y. Simmons, *Spin-orbit coupling in silicon for electrons bound to donors*, npj Quantum Inf. **4**, 61 (2018).

[24] Y. Noda, K. Ohno, and S. Nakamura, *Momentum-dependent band spin splitting in semiconducting* MnO_2*: A density functional calculation*, Phys. Chem. Chem. Phys. **18**, 13294 (2016).

[25] A. Zunger, *Inverse design in search of materials with target functionalities*, Nat. Rev. Chem. **2**, 0121 (2018).

[26] L. D. Yuan, Z. Wang, J. W. Luo, and A. Zunger, *Prediction of low-Z collinear and noncollinear antiferromagnetic compounds having momentum-dependent spin splitting even without spin-orbit coupling*, Phys. Rev. Mater. **5**, 014409 (2021).

[27] W. Kohn and L. J. Sham, *Self-consistent equations including exchange and correlation effects*, Phys. Rev. **140**, A1133 (1965).

[28] G. Kresse and J. Furthmuller, *Efficiency of ab-initio total energy calculations for metals and semiconductors using a plane-wave basis set*, Comput. Mater. Sci. **6**, 15 (1996).

[29] G. Kresse and J. Furthmuller, *Efficient iterative schemes for ab initio total-energy calculations using a plane-wave basis set*, Phys. Rev. B **54**, 11169 (1996).

[30] S. Zeng and Y. J. Zhao, *Description of two-dimensional altermagnetism: Categorization using spin group theory*, Phys. Rev. B **110**, 054406 (2024).

[31] S. K. Zeng and Y. J. Zhao, *Bilayer stacking-type altermagnet: A general approach to generating two-dimensional altermagnetism*, Phys. Rev. B **110**, 174410 (2024).

[32] S. W. Cheong and F. T. Huang, *Altermagnetism classification*, npj Quantum Mater. **10**, 38 (2025).

[33] See Supplemental Material at http://link.aps.org/supplemental/10.1103/mrzv-wmcf for the supplemental computational results on the identified candidate NRSS materials. The Supplemental Material introduced the differences between two classifications of using magnetic point group (SST) vs spin Laue group, and showed the details of theoretical methods used in this work.

[34] M. Gu, Y. Liu, H. Zhu, K. Yananose, X. Chen, Y. Hu, A. Stroppa, and Q. Liu, *Ferroelectric switchable altermagnetism*, Phys. Rev. Lett. **134**, 106802 (2025).

[35] MAGNDATA: https://www.cryst.ehu.es/magndata/index.php?show_db=1.

[36] J. P. Perdew, K. Burke, and M. Ernzerhof, *Generalized gradient approximation made simple*, Phys. Rev. Lett. **77**, 3865 (1996).

[37] S. L. Dudarev, G. A. Botton, S. Y. Savrasov, C. J. Humphreys, and A. P. Sutton, *Electron-energy-loss spectra and the structural stability of nickel oxide: An* LSDA + U *study*, Phys. Rev. B **57**, 1505 (1998).

[38] Materials Project: https://next-gen.materialsproject.org/.

[39] V. Stevanovic, S. Lany, X. W. Zhang, and A. Zunger, *Correcting density functional theory for accurate predictions of compound enthalpies of formation: Fitted*

elemental-phase reference energies, Phys. Rev. B **85**, 115104 (2012).
[40] L. D. Yuan, A. B. Georgescu, and J. M. Rondinelli, *Nonrelativistic spin splitting at the Brillouin zone center in compensated magnets*, Phys. Rev. Lett. **133**, 216701 (2024).
[41] P. F. Liu, J. Y. Li, J. Z. Han, X. G. Wan, and Q. H. Liu, *Spin-group symmetry in magnetic materials with negligible spin-orbit coupling*, Phys. Rev. X **12**, 021016 (2022).
[42] X. B. Chen *et al.*, *Enumeration and representation theory of spin space groups*, Phys. Rev. X **14**, 031038 (2024).
[43] C. Darie, C. Goujon, M. Bacia, H. Klein, P. Toulemonde, P. Bordet, and E. Suard, *Magnetic and crystal structures of* $BiCrO_3$, Solid State Sci. **12**, 660 (2010).
[44] E. Solana-Madruga, A. J. Dos Santos-García, A. M. Arévalo-López, D. Avila-Brande, C. Ritter, J. P. Attfield, and R. Sáez-Puche, *High pressure synthesis of polar and non-polar cation-ordered polymorphs of* Mn_2ScSbO_6, Dalton Trans. **44**, 20441 (2015).
[45] J. L. Garcia-Munoz, J. Rodriguez-Carvajal, X. Obradors, M. Valletregi, J. Gonzalezcalbet, and M. Parras, *Complex magnetic-structures of the rare-earth cuprates* $R_2Cu_2O_5$ *(*R = Y, Ho, Er, Yb, Tm*)*, Phys. Rev. B **44**, 4716 (1991).
[46] J. W. Stout and S. A. Reed, *The crystal structure of* MnF_2, FeF_2, CoF_2, NiF_2 *and* ZnF_2, J. Am. Chem. Soc. **76**, 5279 (1954).
[47] J. Strempfer, U. Rütt, and W. Jauch, *Absolute spin magnetic moment of* FeF_2 *from high energy photon diffraction*, Phys. Rev. Lett. **86**, 3152 (2001).
[48] Y. Fang, W. P. Zhou, S. M. Yan, R. Bai, Z. H. Qian, Q. Y. Xu, D. H. Wang, and Y. W. Du, *Magnetic-field-induced dielectric anomaly and electric polarization in* $Mn_4Nb_2O_9$, J. Appl. Phys. **117**, 17b712 (2015).
[49] M. R. Li *et al.*, *A polar corundum oxide displaying weak ferromagnetism at room temperature*, J. Am. Chem. Soc. **134**, 3737 (2012).
[50] K. Momma and F. Izumi, *For three-dimensional visualization of crystal, volumetric and morphology data*, J. Appl. Crystallogr. **44**, 1272 (2011).
[51] H. van Leuken and R. A. de Groot, *Half-metallic antiferromagnets*, Phys. Rev. Lett. **74**, 1171 (1995).
[52] Y. Liu, S.-D. Guo, Y. Li, and C.-C. Liu, *Two-dimensional fully compensated ferrimagnetism*, Phys. Rev. Lett. **134**, 116703 (2025).
[53] W. N. Lin *et al.*, *Interface-based tuning of Rashba spin-orbit interaction in asymmetric oxide heterostructures with 3D electrons*, Nat. Commun. **10**, 3052 (2019).
[54] O. Fedchenko *et al.*, *Observation of time-reversal symmetry breaking in the band structure of altermagnetic* RuO_2, Sci. Adv. **10**, eadj4883 (2024).
[55] H. Bai *et al.*, *Efficient spin-to-charge conversion via altermagnetic spin splitting effect in antiferromagnet* RuO_2, Phys. Rev. Lett. **130**, 216701 (2023).
[56] S. Lee *et al.*, *Broken Kramers degeneracy in altermagnetic* MnTe, Phys. Rev. Lett. **132**, 036702 (2024).
[57] J. Krempasky *et al.*, *Altermagnetic lifting of Kramers spin degeneracy*, Nature (London) **626**, 517 (2024).
[58] Z. X. Feng *et al.*, *An anomalous Hall effect in altermagnetic ruthenium dioxide*, National electronics review **5**, 735 (2022).
[59] C. T. Liao, Y. C. Wang, Y. C. Tien, S. Y. Huang, and D. R. Qu, *Separation of inverse altermagnetic spin-splitting effect from inverse spin Hall effect in* RuO_2, Phys. Rev. Lett. **133**, 056701 (2024).
[60] T. Aoyama and K. Ohgushi, *Piezomagnetic properties in altermagnetic* MnTe, Phys. Rev. Mater. **8**, L041402 (2024).
[61] T. Osumi, S. Souma, T. Aoyama, K. Yamauchi, A. Honma, K. Nakayama, T. Takahashi, K. Ohgushi, and T. Sato, *Observation of a giant band splitting in altermagnetic* MnTe, Phys. Rev. B **109**, 115102 (2024).
[62] I. I. Mazin, *Altermagnetism in* MnTe*: Origin, predicted manifestations, and routes to detwinning*, Phys. Rev. B **107**, L100418 (2023).
[63] Z. Lin *et al.*, *Observation of giant spin splitting and d-wave spin texture in room temperature altermagnet* RuO_2, arXiv:2402.04995.
[64] Y. Q. Guo *et al.*, *Direct and inverse spin splitting effects in altermagnetic* RuO_2, Adv. Sci. **11**, 2400967 (2024).
[65] P. Wadley *et al.*, *Electrical switching of an antiferromagnet*, Science **351**, 587 (2016).
[66] E. Solana-Madruga, C. Ritter, C. Aguilar-Maldonado, O. Mentré, J. P. Attfield, and A. M. Arévalo-López, $Mn_3MnNb_2O_9$*: High-pressure triple perovskite with* 1:2 *B-site order and modulated spins*, Chem. Commun. (Cambridge) **57**, 8441 (2021).
[67] N. D. Mermin, *Thermal properties of the inhomogeneous electron gas*, Phys. Rev. **137**, A1441 (1965).
[68] P. Blonski and J. Hafner, *Magnetic anisotropy of transition-metal dimers: Density functional calculations*, Phys. Rev. B **79**, 224418 (2009).
[69] P. A. McClarty and J. G. Rau, *Landau theory of altermagnetism*, Phys. Rev. Lett. **132**, 176702 (2024).
[70] I. Turek, *Altermagnetism and magnetic groups with pseudoscalar electron spin*, Phys. Rev. B **106**, 094432 (2022).
[71] L. Attias, A. Levchenko, and M. Khodas, *Intrinsic anomalous Hall effect in altermagnets*, Phys. Rev. B **110**, 094425 (2024).
[72] K. D. Belashchenko, *Exchange-driven spin Hall effect in anisotropic ferromagnets*, Phys. Rev. B **109**, 054409 (2024).
[73] B. Chi, L. Jiang, Y. Zhu, G. Q. Yu, C. H. Wan, and X. F. Han, *Anisotropic spin filtering by an altermagnetic barrier in magnetic tunnel junctions*, arXiv:2409.03415.
[74] K. Samanta, D.-F. Shao, and E. Y. Tsymbal, *Spin filtering with insulating altermagnets*, arXiv:2409.00195.
[75] X. K. Duan, J. Y. Zhang, Z. Y. Zhu, Y. T. Liu, Z. Y. Zhang, I. Zutic, and T. Zhou, *Antiferroelectric altermagnets: Antiferroelectricity alters magnets*, Phys. Rev. Lett. **134**, 106801 (2025).
[76] H. Mavani, K. Huang, K. Samanta, and E. Y. Tsymbal, *Two-dimensional antiferromagnets with non-relativistic spin splitting switchable by electric polarization*, arXiv:2503.09877.
[77] C. Li *et al.*, *Topological Weyl altermagnetism in CrSb*, arXiv:2405.14777.

[78] Q. H. Liu, X. Dai, and S. Blügel, *Different facets of unconventional magnetism*, Nat. Phys. **21**, 329 (2025).

[79] Z. Wang, Y. Sun, X. Q. Chen, C. Franchini, G. Xu, H. Weng, X. Dai, and Z. Fang, *Dirac semimetal and topological phase transitions in* A_3Bi *(*$A = Na, K, Rb$*)*, Phys. Rev. B **85**, 195320 (2012).

[80] Z. J. Wang, H. M. Weng, Q. S. Wu, X. Dai, and Z. Fang, *Three-dimensional Dirac semimetal and quantum transport in* Cd_3As_2, Phys. Rev. B **88**, 125427 (2013).

[81] S. Rajpurohit, R. Karaalp, Y. Ping, L. Z. Tan, T. Ogitsu, and P. E. Blöchl, *Optical control of spin-splitting in an altermagnet*, arXiv:2409.17718.